Field enhancement in hydrogen storage by periodic layered structures

Houria Hamouche[1*], Mohammed M Shabat[2,3] and Guillaume Zoppi[3]
[1]Centre de Développement des Energies Renouvelables, CDER,
BP 62 Route de l'Observatoire, Bouzaréah,16340, Algiers, Algeria
[2]Department of Physics, The Islamic University of Gaza, P.O. Box 108, Gaza Strip, Palestine
[3]Department of Mathematics, Physics & Electrical Engineering, Northumbria University,
Newcastle upon Tyne, NE1 8ST, United Kingdom
*houria.hamouche@gmail.com

Abstract

This paper investigates, through the field enhancement factor, the increase of hydrogen adsorption around the interface between a layer of hydrogen and a periodic layered structure under different incidence angles of an applied transverse magnetic polarized electromagnetic field. This periodic layered structurel is composed of n-binary unit cells based on alternating a thin layer of gold with a thin layer of a metamaterial with equal negative relative permittivity while the relative permeability of the first and the second material's unit cell is considered equal to 1 and -1, respectively. We apply the effective medium theory to replace this layered structure with a single slab of a homogeneous material with an effective permittivity tensor and an effective permeability tensor. We use the Transfer Matrix Method to analyze the reflectivity spectra at the hydrogen/slab interface for adjustable layers' thicknesses and then we derive the field enhancement factor. We obtain a significant increase of the field enhancement factor of the structure in comparison with the field enhancement factor around the interface between a layer of hydrogen and a structure composed of one gold layer.

Keywords: Periodic, Metamaterial, Reflectivity, Field enhancement factor, Effective medium theory, Transfer matrix method.

1. Introduction

The harnessing of the energy stored in hydrogen to produce electrical energy encounters several difficulties, among which the lack of efficient storage methods is the most critical [1-10]. There are many ways to store hydrogen, including pressurized gas, liquefied, and material-based methods [11-17]. The high-pressure gas and the cryogenic liquid methods suffer from different limitations such as safety, efficiency, poor volumetric energy density, and high cost of the storage process [18-19]. Currently, the most promising means to store hydrogen is using solid-state materials [20-21]. However, due to the weak interaction between hydrogen and the surface of solid materials, no significant amount of hydrogen can be stored at ambient temperature and pressure [22, 23]. Metal hydrides result from the interaction of hydrogen with a metal surface

[24-27] as hydrogen storage materials and are often preferred over conventional storage methods because of their gravimetric and volumetric storage capacities and safe operating pressures [28-31]. Nonetheless, the slow absorption/desorption kinetics of bulk metal hydrides remains the major disadvantage of metal hydride systems [32-34]. During the last few decades, hydrogen storage in nanostructured materials with high hydrogen storage capacity in a reversible way has attracted increasing attention [35-38]. Nanostructured materials include multiple structures such as nanoparticles, nanoconfined composites, core-shell structures, nanowires, nanotubes, thin films, and multilayers [39-42]. The advantages of thin-film metal hydrides have been discussed by Baldi and Dam [43]. Films of Au and Pd at different intermixing ratios, as well as layered Au/Pd films deposited in an alternating fashion have been used by Nishijima *et al.* for prospective applications in hydrogen detection and storage [44]. The adsorption of hydrogen on gold nanoparticles of the size of the order of 10 nm has been investigated by Watkins and Borensztein [45]. To achieve high performance with high hydrogen-absorbing capacity and suitable absorption/desorption temperature, a design of nanocomposite hydrogen-absorbing material has been proposed by Higuchi *et al.* [46, 47]. The improvement of the hydrogen adsorption by an applied electromagnetic field has been examined by several researchers. An investigation of the interaction and kinetics of hydride forming materials under high-frequency electromagnetic fields has been undertaken by Bell [48]. The effects of electric field strength on hydrogen adsorption have been determined by Hwang *et al*. [49]. Borgschulte *et al.* have used an electric current to control the absorption of hydrogen in Mg thin films [50]. Song *et al.* have shown that an appropriate external electric field can effectively enhance the hydrogen adsorption/desorption on the Ca–silicene system [51]. The high-performance unidirectional absorber structure of conventional dielectrics and graphene layers has been realized by Guo *et al.* [52]. The optical bistability of one-dimensional photonic crystals has been reported by Xu *et al.* [53]. Surface-plasmon-induced electromagnetic field enhancement around planar surfaces of hydrogen-absorbing transition metals has been quantitatively investigated by Fukuoka and Tanabe [54].

In this work, we numerically analyze the field enhancement factor around the interface between a layer of hydrogen and several periodic layered structures composed of n-binary unit cells based on alternating gold and metamaterial layers in the quest to improve the interaction around the interface under an incident electromagnetic field. Periodic layered structures, when plasma is considered as a kind of metamaterial, are similar to plasma photonic crystal structures [55, 56]. Metamaterials also referred to as Left-Handed Materials (LHM) following the original term proposed by Veselago [57, 58], are defined as materials whose properties depend strongly on

the geometry of the microstructure [59, 60]. Negative relative electric permittivity and negative relative magnetic permeability, in certain wavelength region, are one of the most important optical properties of metamaterials [61-63].

By applying the effective medium theory, which allows by replacing a periodic layered structure with a single homogeneous material slab, the slab effective permittivity tensor and the slab effective permeability tensor are determined. The reflectivity spectra of both a normal incident electromagnetic field and a transverse magnetic polarized electromagnetic field under different incidence angles at the hydrogen/slab interface are calculated by the Transfer Matrix Method. The dependence of the field enhancement factor on the layers' thicknesses, on the number of periods, and the incidence angles is discussed.

2. Theoretical formulation

2.1. Effective permittivity and permeability tensors

This work deals with the field enhancement factor around the hydrogen/gold slab interface and the field enhancement factor around hydrogen/periodic layered structures interfaces for wavelengths from 500 nm to 2100 nm. The periodic layered structure is composed of n-binary unit cells based on alternating gold and metamaterial layers with the same negative relative permittivity. The relative permeability of gold and the metamaterial is considered equal to 1 and -1, respectively. In this study, the Drude model is used to express the relative electric permittivity $\varepsilon_{met}(\omega)$ [64, 65]

$$\varepsilon_{met}(\omega) = \varepsilon_{lattice} - \frac{\omega_p^2}{\omega^2 + i.\gamma.\omega} \qquad (1)$$

where $\varepsilon_{lattice}$ is the lattice permittivity, ω_p is the plasma frequency and γ is the scattering rate. Values of $\varepsilon_{lattice}$, ω_p and γ are those given by Isaac *et al.* [65]: $\varepsilon_{lattice} = 9.1$, $\omega_p = 1.2 * 10^{16}$ rad/s and $\gamma = 1.2 * 10^{14}$ rad/s. The complex relative electric permittivity is presented in Fig.1.

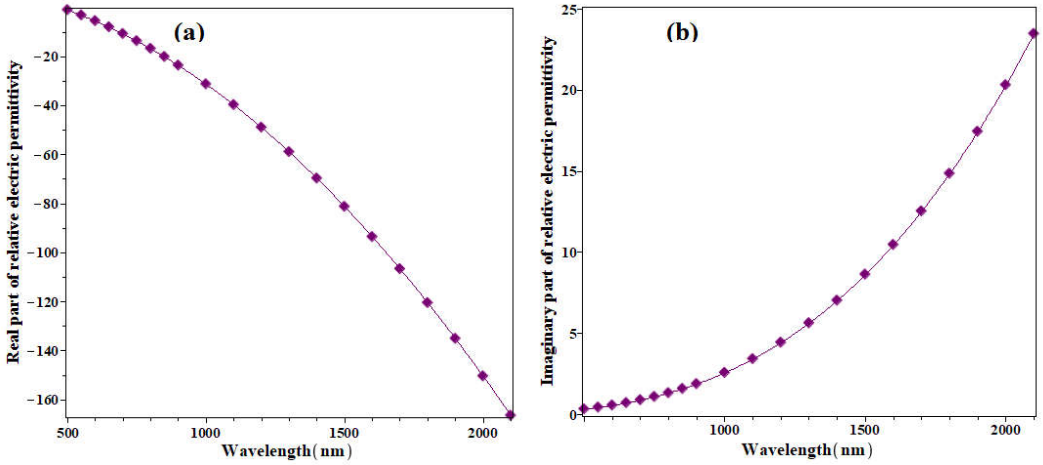

Fig. 1. Complex relative electric permittivity versus wavelength. (a) real part and (b) imaginary part.

.

The effective medium theory simplified a periodic layered structure to a one-layer homogeneous medium with an effective diagonal permittivity tensor and an effective diagonal permeability tensor when the thickness of each layer of the structure d_i is much smaller than the wavelength of the incident electromagnetic field in the effective medium given by λ/n_{eff} (λ is the wavelength and n_{eff} is the effective refractive index of the medium) [66]. The effective permittivity tensor ε_{eff} and the effective permeability tensor μ_{eff} are written as [67-71]

$$\varepsilon_{eff} = \begin{bmatrix} \varepsilon_{eff}^{\parallel} & 0 & 0 \\ 0 & \varepsilon_{eff}^{\parallel} & 0 \\ 0 & 0 & \varepsilon_{eff}^{\perp} \end{bmatrix} \text{ and } \mu_{eff} = \begin{bmatrix} \mu_{eff}^{\parallel} & 0 & 0 \\ 0 & \mu_{eff}^{\parallel} & 0 \\ 0 & 0 & \mu_{eff}^{\perp} \end{bmatrix} \qquad (2)$$

The diagonal components $\varepsilon_{eff}^{\parallel}$, $\varepsilon_{eff}^{\perp}$, $\mu_{eff}^{\parallel}$ and $\mu_{eff}^{\perp}$ are given by

$$\varepsilon_{eff}^{\parallel} = \sum \varepsilon_i . \frac{d_i}{d},\ \frac{1}{\varepsilon_{eff}^{\perp}} = \sum \frac{1}{\varepsilon_i} . \frac{d_i}{d},\ \mu_{eff}^{\parallel} = \sum \mu_i . \frac{d_i}{d} \text{ and } \frac{1}{\mu_{eff}^{\perp}} = \sum \frac{1}{\mu_i} . \frac{d_i}{d} \qquad (3)$$

with ε_i, μ_i, d_i the relative permittivity, the relative permeability and the thickness of each layer of the unit cell, respectively. The thickness of the unit cell is given by d ($d = \sum d_i$). For unit cell materials with the same relative permittivity ε_{met} , the diagonal components of the effective permittivity tensor are equal to ε_{met} ($\varepsilon_{eff}^{\parallel} = \varepsilon_{eff}^{\perp} = \varepsilon_{met}$). For binary unit cell materials with the first material relative permeability equal to 1 and the second material relative permeability equal to -1, the diagonal components of the effective permeability tensor are calculated by

$$\mu_{eff}^{\parallel} = \frac{d_{met} - d_{LHM}}{d_{met} + d_{LHM}},\ \mu_{eff}^{\perp} = \frac{d_{met} + d_{LHM}}{d_{met} - d_{LHM}} \qquad (4)$$

where d_{met} and d_{LHM} are the thicknesses of the first and second materials, respectively.

2.2. Field enhancement factor theory

Metal nanostructures can interact strongly with electromagnetic fields or light of wavelength significantly exceeding their dimensions due to their ability to support surface plasmons. Surface plasmons are the excitations of collective oscillations of free electrons confined within the interface of the metal and the dielectric, accompanied by strong field enhancement at the subwavelength scale [72, 73]. Near surfaces or interfaces, the electromagnetic field can alter the motion of charged particles and improve reactions kinetics [48]. The field enhancement can be studied via the field enhancement factor which is defined as the intensity ratio for electric field around the metal ($\overrightarrow{E_{SP}}(0^+)$ to that in the absence of the metal, or the incident electric field ($\overrightarrow{E_0}$) . The field enhancement factor η is expressed by [54, 74-76]

$$\eta = \frac{\left|\overrightarrow{E_{SP}}(0^+)\right|^2}{\left|\overrightarrow{E_0}\right|^2} = \frac{\lambda.(|q_1|^2+|k_{SP}|^2).(1-R).cos\,\theta}{2.\pi.\varepsilon_1^{1/2}.k''_{SP}.Re\{\frac{k_{SP}.(\varepsilon_1.q'_1+\varepsilon_2.q'_2)}{\varepsilon_2.q'_1.q'_2}\}} \quad (5)$$

where λ is the wavelength of the field related to the frequency of the field ω by $\lambda = \frac{2.\pi.c}{\omega}$, c is the speed of light; θ is the incident angle; R is the reflectivity of the incident field; q_1 and q_2 are the complex wave vectors in the z-direction in the hydrogen layer and the material slab, respectively; k_{SP} is the complex wave vector of the surface-plasmon mode in the x-direction. The primes and double primes indicate the real and imaginary parts of complex quantities, respectively. Based on the derivation of the dispersion relation developed by Weber [74] and Raether [72], the wave vectors have been calculated for both normal incident field and transverse magnetic polarized field.

For the normal incident field, the dispersion relations are given by

$$q_1^2 = {k_{SP}}^2 - \mu_1.\varepsilon_1.\left(\frac{2.\pi}{\lambda}\right)^2, \qquad q_2^2 = {k_{SP}}^2 - \mu_{eff}^{\parallel}.\varepsilon_{eff}^{\parallel}.\left(\frac{2.\pi}{\lambda}\right)^2 \quad (6)$$

For the transverse magnetic polarized field, the dispersion relations are given by

$$q_1^2 = {k_{SP}}^2 - \mu_1.\varepsilon_1.\left(\frac{2.\pi}{\lambda}\right)^2, \qquad q_2^2 = {k_{SP}}^2 - \mu_{eff}^{\parallel}.\varepsilon_{eff}^{\perp}.\left(\frac{2.\pi}{\lambda}\right)^2 \quad (7)$$

For the case of this study, the permittivity and the permeability of hydrogen are taken equal to 1 ($\varepsilon_1 = \mu_1 = 1$) and as the diagonal components of the effective permittivity tensor are equal, the dispersion relations remain the same for normal and transverse magnetic polarized fields. The wave complex vectors have been deduced from these dispersion relations as

$$q_1 = \frac{2.\pi}{\lambda}.\left(\frac{1-\mu_{eff}^{\parallel}.\varepsilon_{eff}^{\parallel}}{{\varepsilon_{eff}^{\parallel}}^2-1}\right)^{1/2}, \quad q_2 = \frac{2.\pi}{\lambda}.\left[\frac{{\varepsilon_{eff}^{\parallel}}^2.(1-\mu_{eff}^{\parallel}.\varepsilon_{eff}^{\parallel})}{{\varepsilon_{eff}^{\parallel}}^2-1}\right]^{1/2} \text{ and } k_{SP} = \frac{2.\pi}{\lambda}.\left[\frac{\varepsilon_{eff}^{\parallel}.(\varepsilon_{eff}^{\parallel}-\mu_{eff}^{\parallel})}{{\varepsilon_{eff}^{\parallel}}^2-1}\right]^{1/2}$$

(8)

The reflectivity of the incident field on the hydrogen/slab interface required for the calculation of the field enhancement factor is performed using the Transfer Matrix Method. Transfer Matrix Method is a very useful and quite simple method for the analysis of the optical parameters of multilayer structures. The transfer matrix relates the incoming and the outgoing waves on the input layer of a structure to those on the output layer [77-81]. The considered structure is composed of a slab of an effective material with an index of refraction n_s embedded in a semi-infinite input hydrogen layer and a semi-infinite output air layer. The slab's refractive index n_s is given by

$$n_s = \begin{cases} \sqrt{\mu_{eff}^{\parallel}.\varepsilon_{eff}^{\parallel}} & \text{for nomal incident electromagnetic field.} \\ \sqrt{\mu_{eff}^{\parallel}.\varepsilon_{eff}^{\perp}} & \text{for transverse magnetic polarised electromagnetic field.} \end{cases} \quad (9)$$

The complete transfer matrix M is obtained by multiplying the individual transfer matrices

$$M = M_H^{-1}.M_s.M_a = \begin{bmatrix} M_{11} & M_{12} \\ M_{21} & M_{22} \end{bmatrix} \quad (10)$$

with

$$M_H = \begin{bmatrix} 1 & 1 \\ n_H^{eff} & -n_H^{eff} \end{bmatrix}, M_a = \begin{bmatrix} 1 & 1 \\ n_a^{eff} & -n_a^{eff} \end{bmatrix} \quad (11)$$

and

$$M_s = \begin{bmatrix} \cos\delta_s & \frac{i\sin\delta_s}{n_s^{eff}} \\ in_s^{eff}\sin\delta_s & \cos\delta_s \end{bmatrix} \quad (12)$$

where n_H and n_a are the refractive indices of hydrogen and air, respectively.

$$n_H = n_a = 1 \quad (13)$$

n_j^{eff} and δ_j , with j=H, s, a, are the effective refractive indices and the phase thicknesses, respectively. Furthermore,

$$n_j^{eff} = \begin{cases} n_j \cos\theta_j & \text{for transverse electric polarisation (TE).} \\ \frac{n_j}{\cos\theta_j} & \text{for transverse magnetic polarisation (TM).} \end{cases} \quad (14)$$

and

$$\delta_j = \frac{2\pi}{\lambda}.n_j.d_j.\cos\theta_j \quad (15)$$

The angle of refraction θ_j is related to the incidence angle θ_0 by the Snell's law

$$n_H.\sin\theta_0 = n_j.\sin\theta_j \quad (16)$$

The reflectivity R is the square of the reflection amplitude r.

$$R = |r|^2 \qquad (17)$$

The reflection amplitude can be written in terms of the transfer matrix coefficients as

$$r = \frac{M_{21}}{M_{11}} \qquad (18)$$

3. Numerical Simulation Results

3.1. Field enhancement factor around hydrogen/gold slab interface

The geometry of the first investigated structure is shown in Fig. 2.(a). In the simulations, an electromagnetic field at normal incidence ($\theta = 0$) is applied on the interface of a semi-infinite hydrogen layer and a gold slab with thickness d_{met}. Fig. 3 includes the presentation of the reflectivity for several gold thicknesses. It can be seen from Fig.3 that the reflectivity increases with the increase of the gold thickness. In contrast to the reflectivity, the field enhancement factor is decreasing. This decrease appears clear in Fig.4. It is also interesting to remark that the field enhancement factor calculated without considering the reflectivity is the highest in all the range of wavelength from 500 nm to 2100 nm.

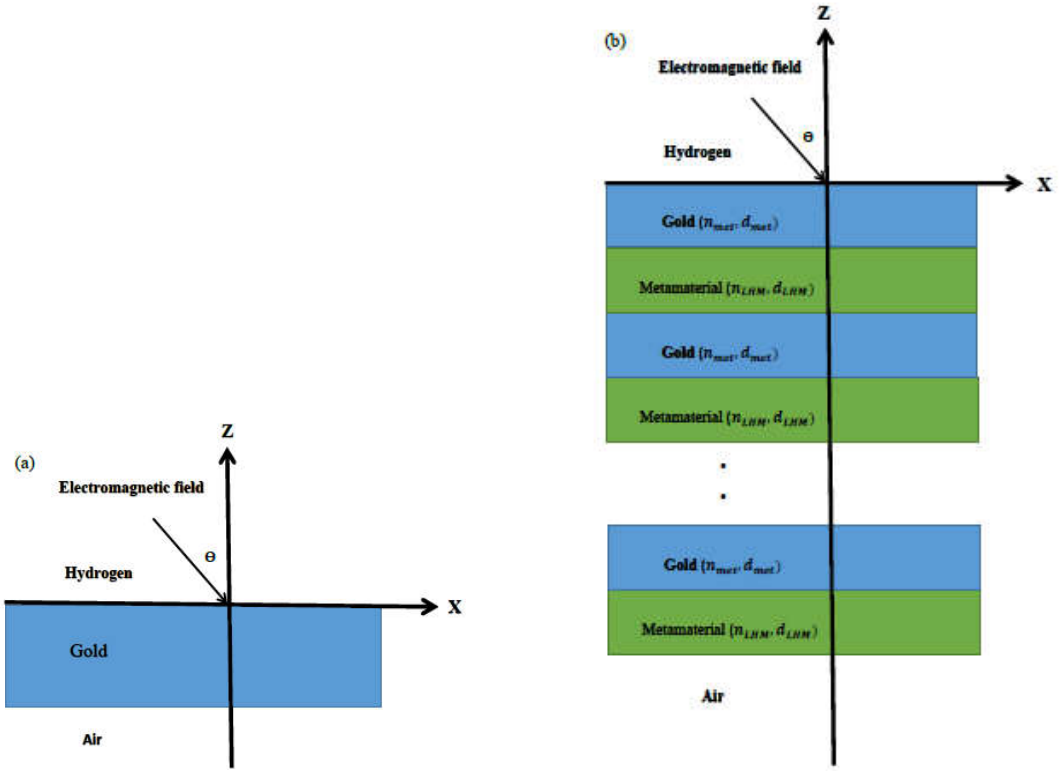

Fig. 2. Schematic diagrams of the proposed structures. (a) structure composed of one gold layer and (b) a periodic layered structure composed of alternating layers of gold and metamaterial

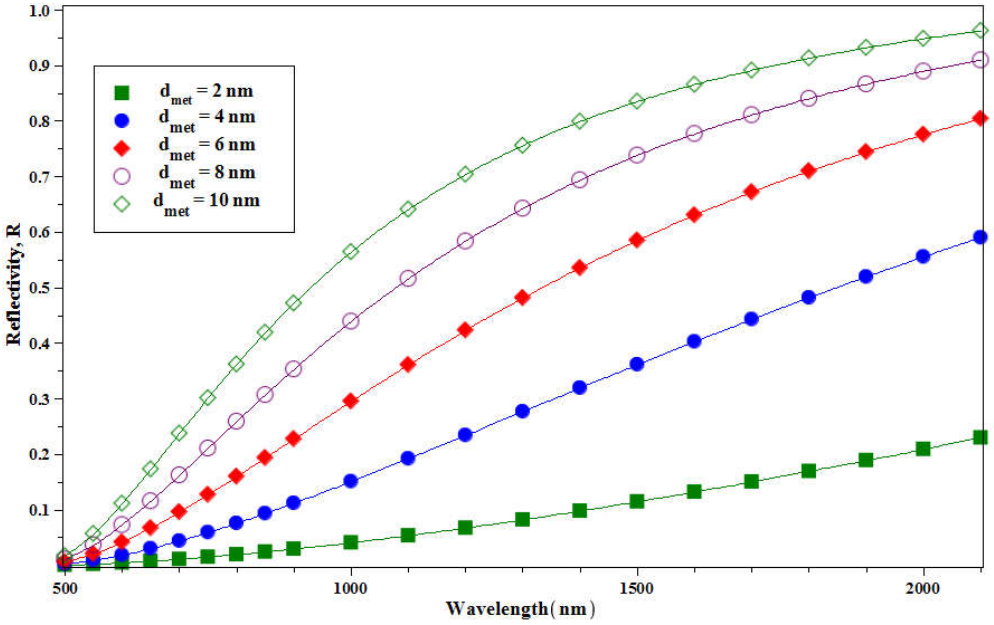

Fig. 3. Reflection under normal incidence around hydrogen/gold slab interface for several gold thicknesses versus wavelength

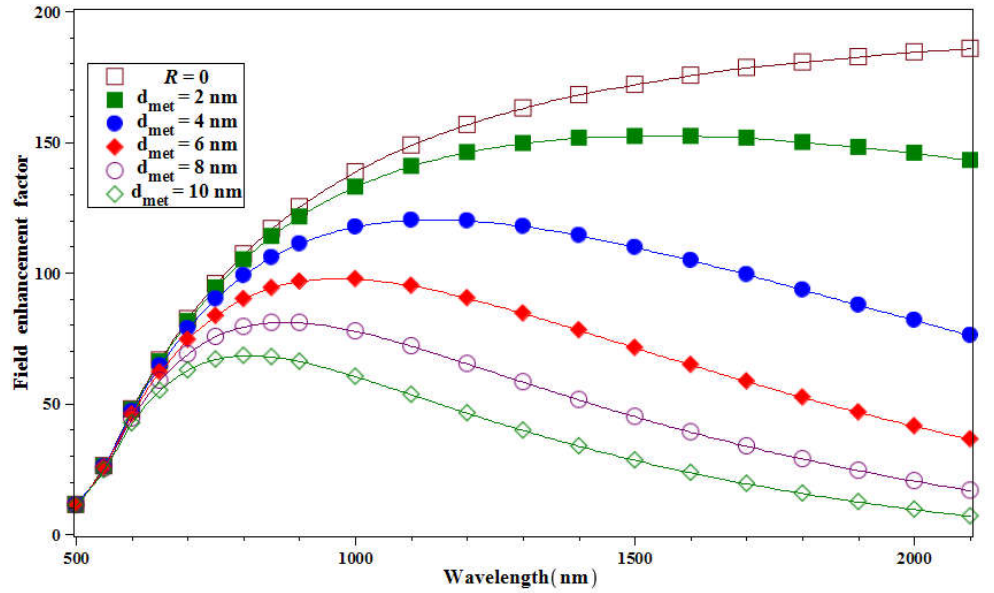

Fig. 4. Field enhancement factors versus wavelength around hydrogen/gold slab interface for several gold thicknesses

3.2. Field enhancement factor around hydrogen/periodic layered structures interfaces

In order to enhance the field enhancement factor, the second type of geometry of structures composed of n-binary unit cell based on alternating a thin layer of gold with a thin layer of metamaterial is proposed. The layered structure of these cells can be seen in Fig. 2 (b). From the thickness dependence of the effective permeability components tensor, the real and the

imaginary parts of the effective slab's refractive index with adjustable gold and metamaterial layers' thicknesses are calculated and depicted in figures Fig.5 (a) and Fig.5 (b). In figure Fig.5 (c) the ratio $Z = \frac{d_i}{\lambda/|n_{eff}|}$ of the thickness of each layer to the wavelength in the effective mediums is plotted versus the wavelength. As can be seen from the figure Fig.5 (c), the maximum values of Z do not exceed 0.8%, 1% and 1.4% for the thicknesses' layers of 6 nm, 10 nm and 20 nm, respectively. Therefore, the effective medium theory is a suitable approach to the proposed structures.

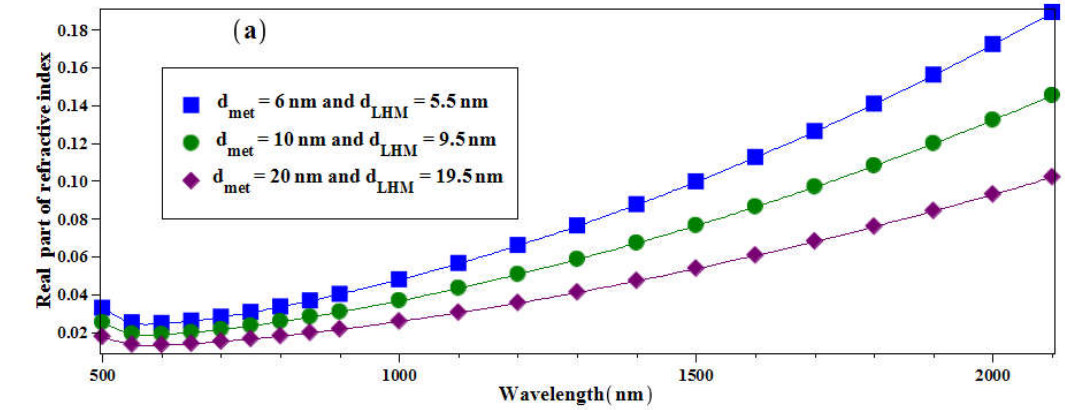

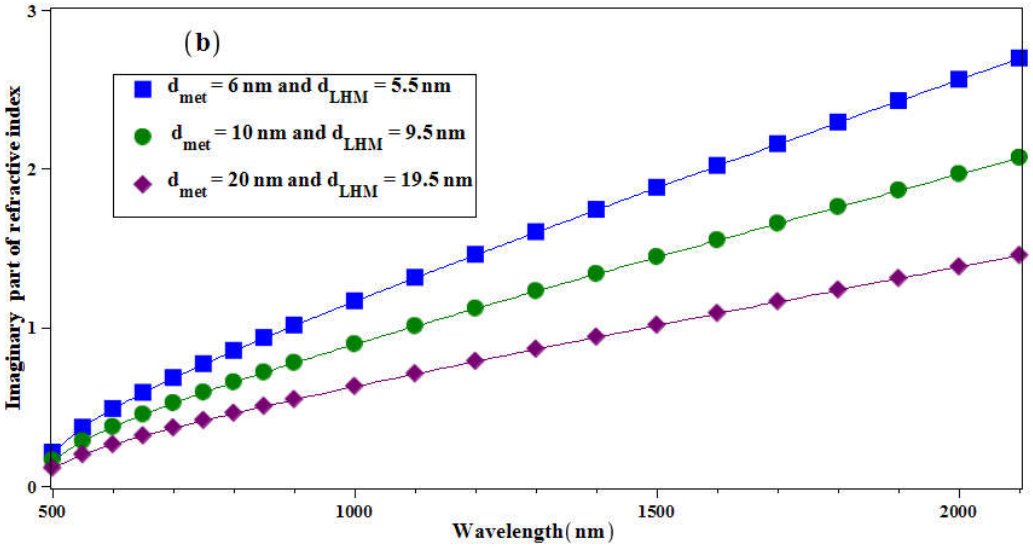

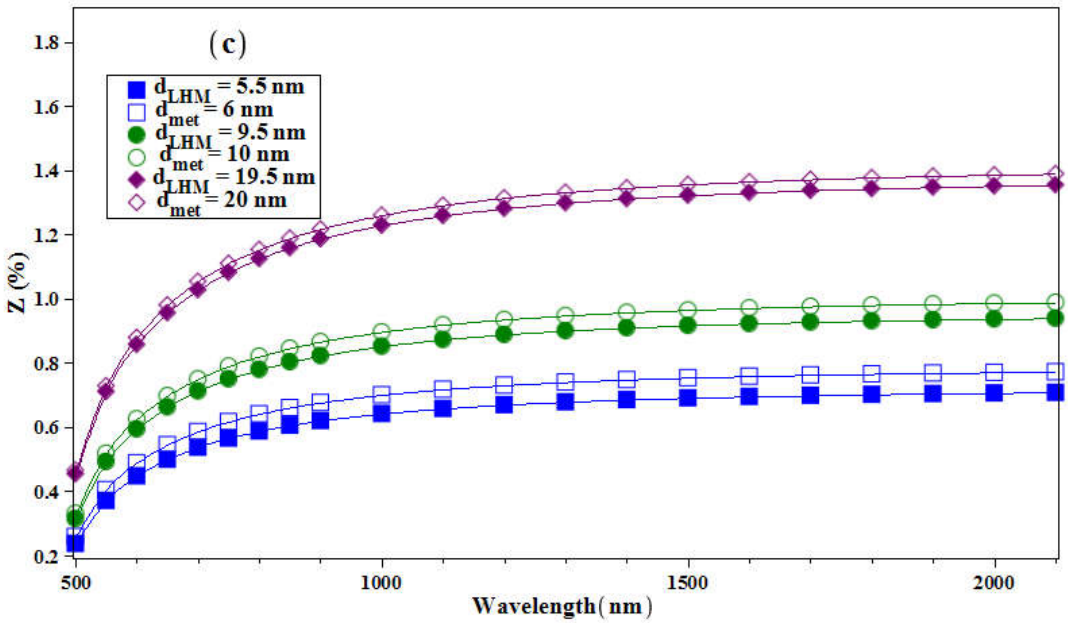

Fig. 5. Complex refractive index of the effective slab versus wavelength. (a) real part and (b) imaginary part. (c) ratio Z versus wavelength

The field enhancement factors under a normal incident electromagnetic field of these three periodic layered structures of n-binary unit cell with $d_{met} = 6\,nm$ and $d_{LHM} = 5.5\,nm$; $d_{met} = 10\,nm$ and $d_{LHM} = 9.5\,nm$ and $d_{met} = 20\,nm$ and $d_{LHM} = 19.5\,nm$, are calculated for $\mathrm{n} = 1, 2, \ldots,$ and 10. The results are plotted in Fig. 6. These figures show a significant increasing of the field enhancement factor of the layered structures in comparison with the field enhancement factor around gold/hydrogen interface (Fig. 4). The obtained results can be summarized as follows. Firstly, reducing the number of periods leads to an increase in the field enhancement factor. Secondly, the reflectivity can be neglected in the calculation of the field enhancement factor only for structures with one unit cell. This can be seen in Fig. 7, which shows nearly zero reflectivity for one unit cell structure. Thirdly, the trend of the curves remains unchanged even though the number of period changes. Fig. 6. (a) shows a continuously increasing of the field enhancement factor with wavelengths for the structure of unit cell with $d_{met} = 6\,nm$ and $d_{LHM} = 5.5\,nm$. The field enhancement factor attains its maximum at 2100 nm. This continuous increase, as it can be seen in Fig. 6. (b) and Fig. 6. (c), is also observed in the range of wavelength from 500 nm to 1400 nm for the two structures of unit cells with $d_{met} = 10\,nm$ and $d_{LHM} = 9.5\,nm$ and $d_{met} = 20\,nm$ and $d_{LHM} = 19.5\,nm$ and an oscillatory increasing behavior characterizes the field enhancement factor in the range of wavelength from 1400 nm to 2100 nm.

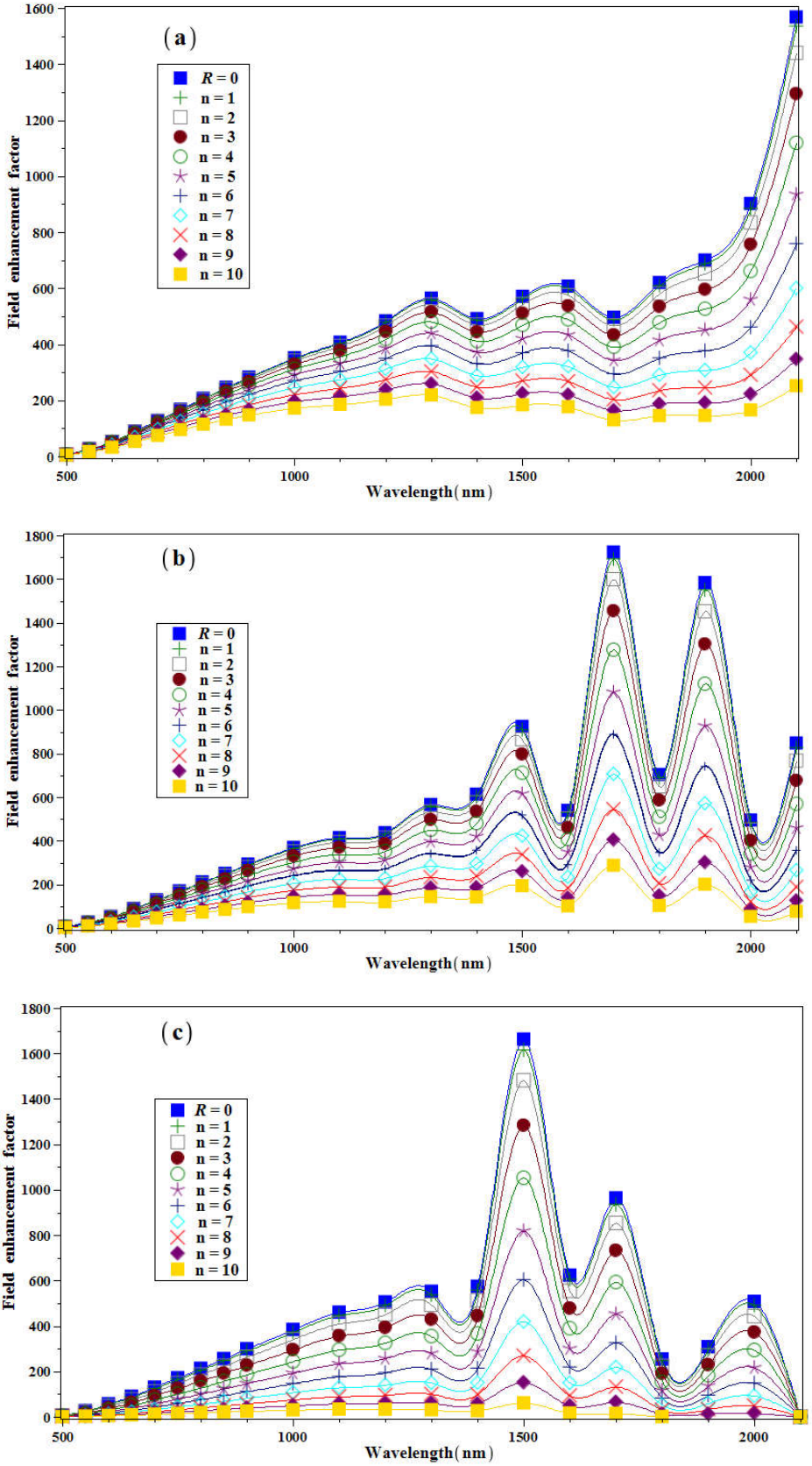

Fig. 6. Field enhancement factors versus wavelength around hydrogen/periodic layered structures interfaces. (a) structure of unit cell with $d_{met} = 6\ nm$ and $d_{LHM} = 5.5\ nm$; (b) structure of unit cell with $d_{met} = 10\ nm$ and $d_{LHM} = 9.5\ nm$; (c) structure of unit cell with $d_{met} = 20\ nm$ and $d_{LHM} = 19.5\ nm$

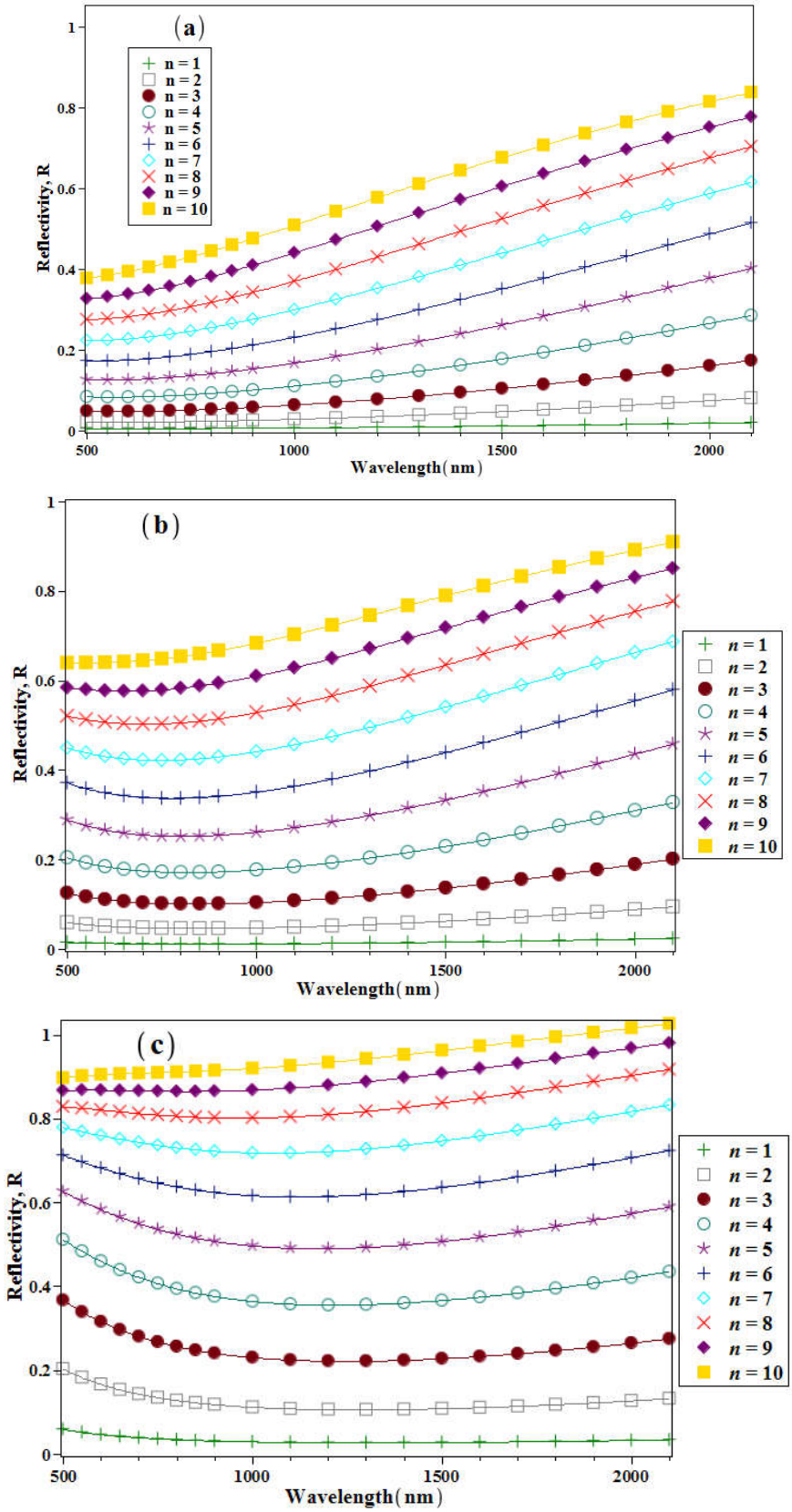

Fig. 7. Reflectivity under normal incidence versus wavelength at hydrogen/periodic layered structures interfaces. (a) structure of unit cell with $d_{met} = 6\ nm$ and $d_{LHM} = 5.5\ nm$; (b) structure of unit cell with $d_{met} = 10\ nm$ and $d_{LHM} = 9.5\ nm$; (c) structure of unit cell with $d_{met} = 20\ nm$ and $d_{LHM} = 19.5\ nm$

3.3. Field enhancement factor under a polarized transverse magnetic electromagnetic field

In this section, we present an analysis of the field enhancement factor around hydrogen/5-binary unit cell layered structure interface under different incidence angles of an applied transverse magnetic polarized electromagnetic field. Fig. 8 illustrates the variation with an incidence angle of the field enhancement factor for the three structures. Through figure Fig. 8 (a) and Fig. 8 (b), the field enhancement factor for the structures of unit cells with $d_{met} = 6\ nm$ and $d_{LHM} = 5.5\ nm$ and $d_{met} = 10\ nm$ and $d_{LHM} = 9.5\ nm$ is shown decreasing as the incidence angles increase. Very little difference is observed between the field enhancement factors under the angles $\theta = 15^0$ and $\theta = 30^0$. The field enhancement factor remains nearly identical under normal incidence ($\theta = 0^0$) and $\theta = 15^0$. Fig. 8 (c) portrays the field enhancement factor for the structure of unit cells with $d_{met} = 20\ nm$ and $d_{LHM} = 19.5\ nm$. No difference is observed in the behavior of the curves of the field enhancement factor under the angles $\theta = 15^0$, $\theta = 30^0$ and $\theta = 45^0$ in the range of wavelength from 1400 nm to 2100 nm. The weakest values in all the range of wavelength (from 500 nm to 2100 nm) are obtained under $\theta = 60^0$. The highest values in the range of wavelength from 750 nm to 1000 nm and from 1000 nm to 1400 nm are obtained under $\theta = 30^0$ and $\theta = 60^0$, respectively.

The results presented in Fig. 8 are combined in Fig. 9 with the simulation results obtained without taking into account the reflectivity, in order to explicit the effect of reflectivity on the field enhancement factor. The curves exhibit a significant difference between the field enhancement factors calculated with and without reflectivity. The curves calculated without reflectivity lie significantly above the curves calculated with considering the reflectivity.

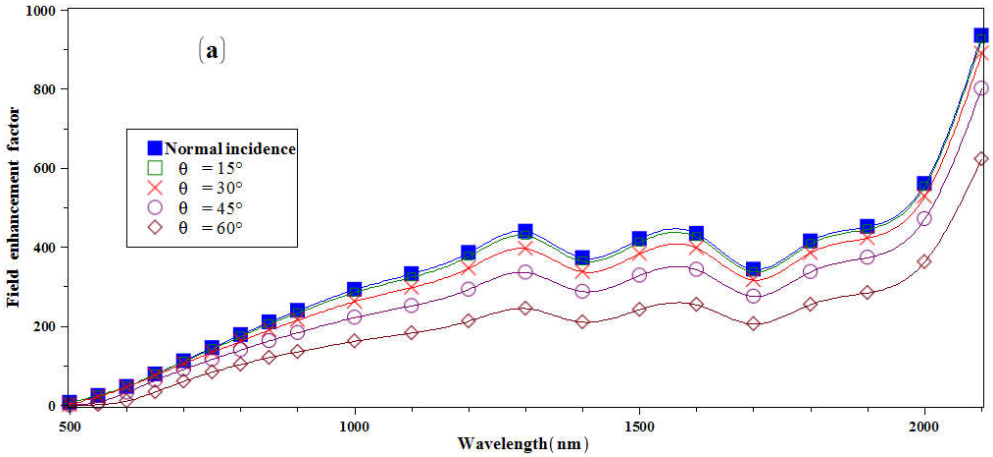

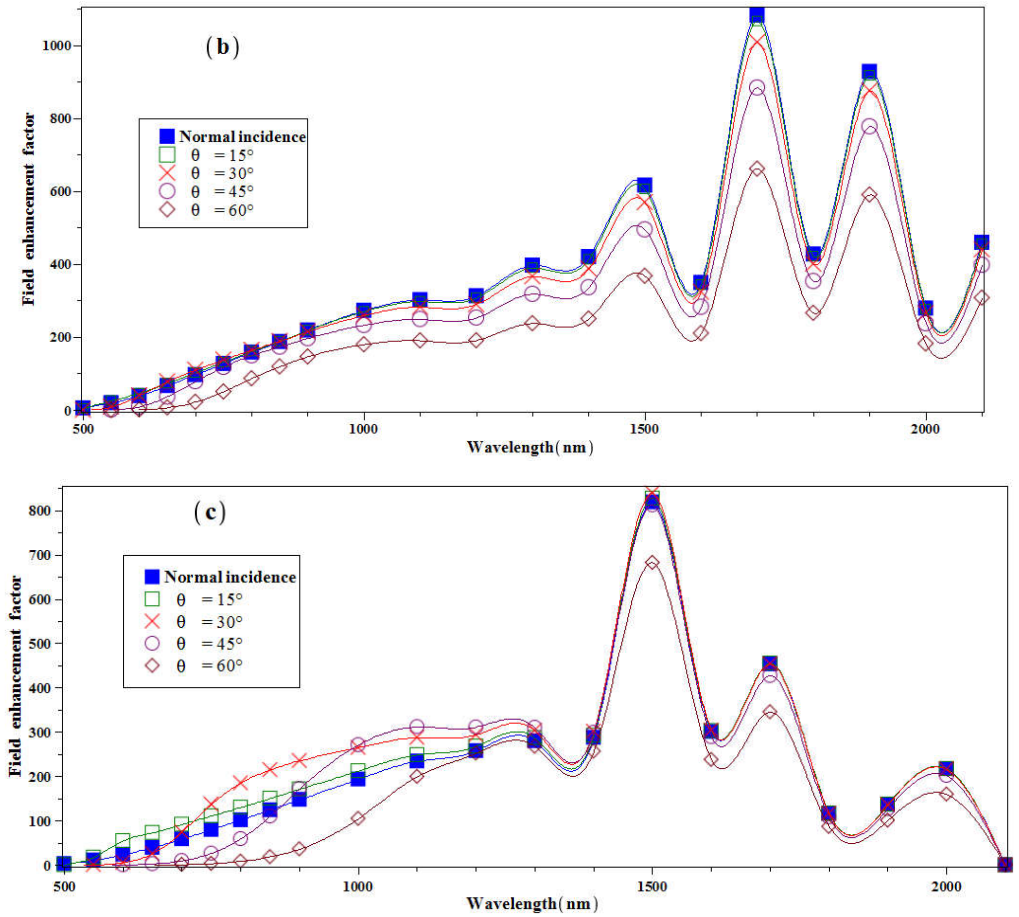

Fig. 8. Field enhancement factors under a transverse magnetic polarized electromagnetic field versus wavelength. (a) structure of unit cell with $d_{met} = 6\ nm$ and $d_{LHM} = 5.5\ nm$; (b) structure of unit cell with $d_{met} = 10\ nm$ and $d_{LHM} = 9.5\ nm$; (c) structure of unit cell with $d_{met} = 20\ nm$ and $d_{LHM} = 19.5\ nm$

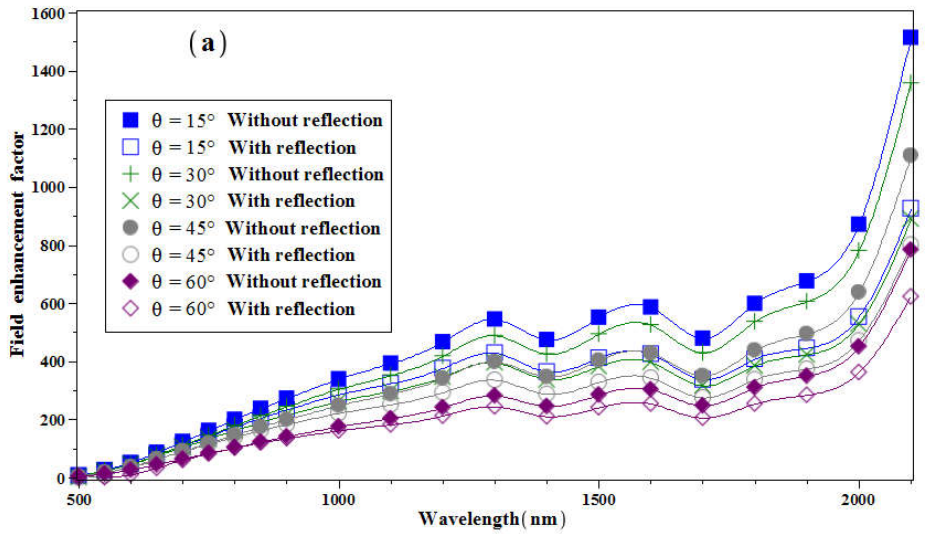

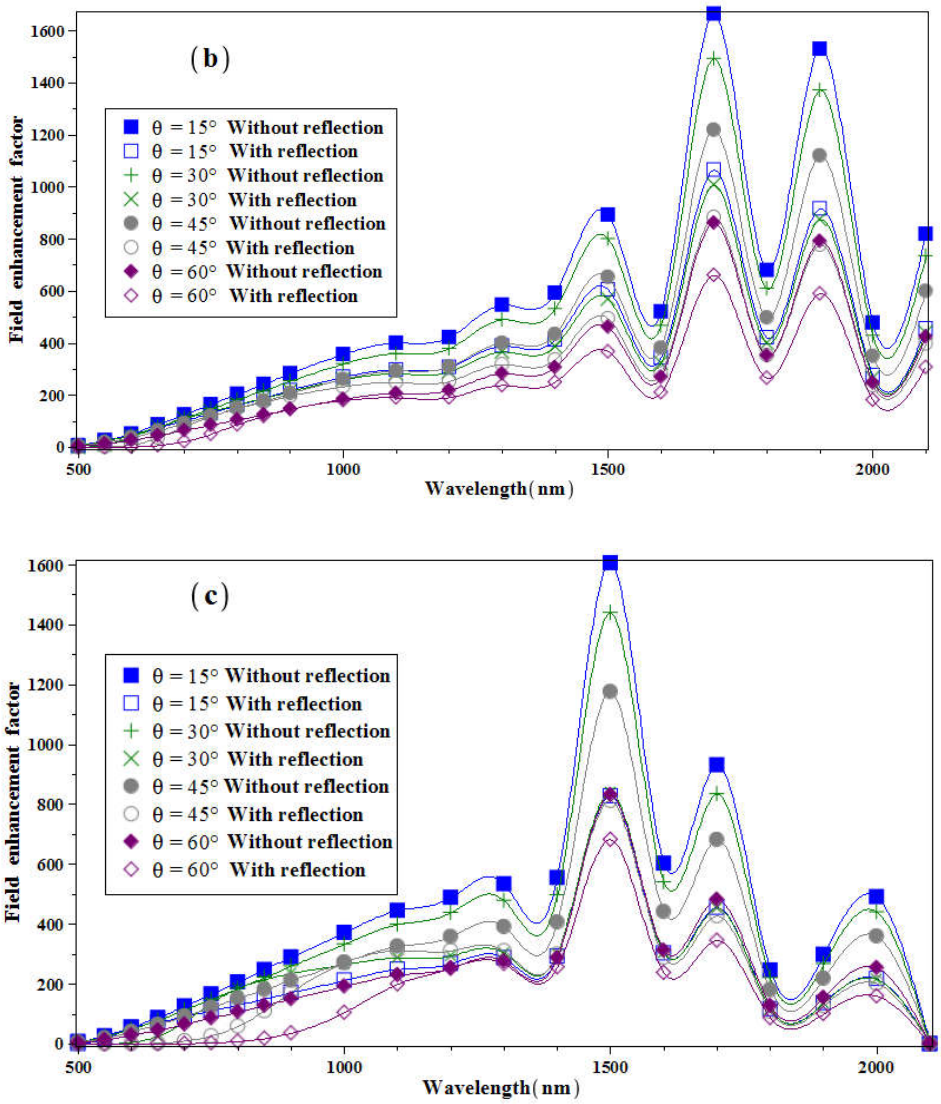

Fig. 9. Field enhancement factors under a transverse magnetic polarized electromagnetic field versus wavelength. (a) structure of unit cell with $d_{met} = 6\ nm$ and $d_{LHM} = 5.5\ nm$; (b) structure of unit cell with $d_{met} = 10\ nm$ and $d_{LHM} = 9.5\ nm$; (c) structure of unit cell with $d_{met} = 20\ nm$ and $d_{LHM} = 19.5\ nm$

In the last part of this paper, we compare the field enhancement factors of the three structures under the same incident angle. Results obtained, presented in Fig.10, indicate no important changes in the values of the field enhancement factors of the structures of unit cells with $d_{met} = 6\ nm$ and $d_{LHM} = 5.5\ nm$ and $d_{met} = 10\ nm$ and $d_{LHM} = 9.5\ nm$, in the range of wavelength from 500 nm to 1400 nm. The highest values of the field enhancement factor are obtained for the structure of unit cells with $d_{met} = 10\ nm$ and $d_{LHM} = 9.5\ nm$, in the range of wavelength from 1400 nm to 1900 nm.

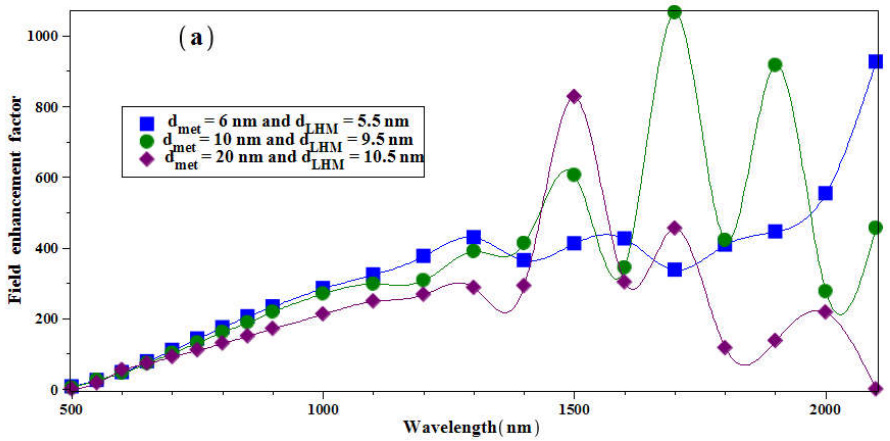
(a)
d_{met} = 6 nm and d_{LHM} = 5.5 nm
d_{met} = 10 nm and d_{LHM} = 9.5 nm
d_{met} = 20 nm and d_{LHM} = 10.5 nm
Field enhancement factor
Wavelength(nm)

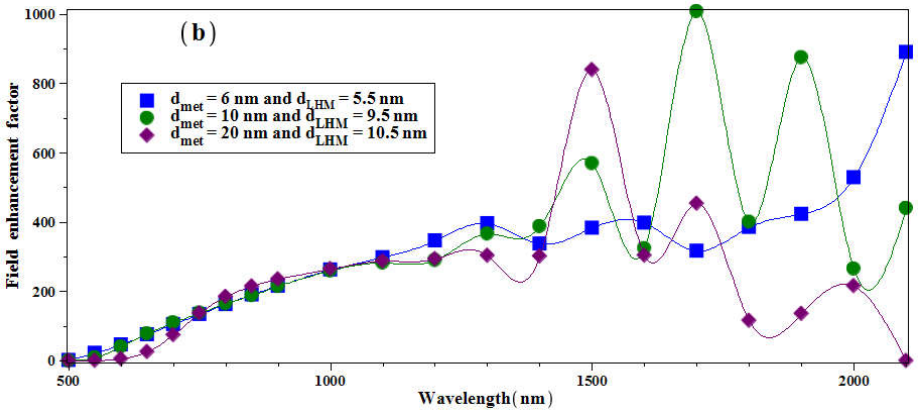
(b)
d_{met} = 6 nm and d_{LHM} = 5.5 nm
d_{met} = 10 nm and d_{LHM} = 9.5 nm
d_{met} = 20 nm and d_{LHM} = 10.5 nm
Field enhancement factor
Wavelength(nm)

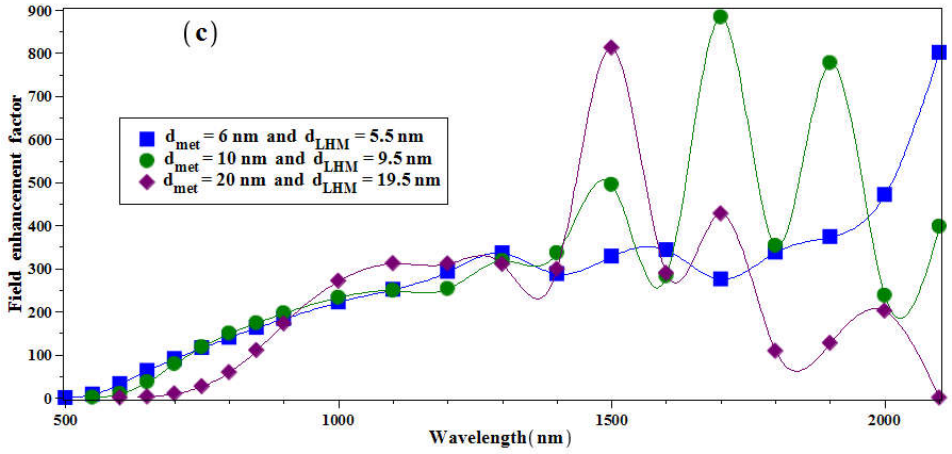
(c)
d_{met} = 6 nm and d_{LHM} = 5.5 nm
d_{met} = 10 nm and d_{LHM} = 9.5 nm
d_{met} = 20 nm and d_{LHM} = 19.5 nm
Field enhancement factor
Wavelength(nm)

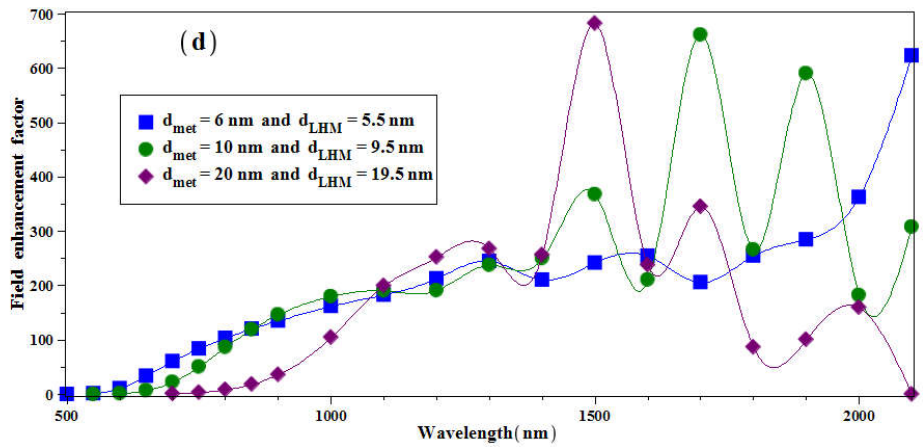
(d)
d_{met} = 6 nm and d_{LHM} = 5.5 nm
d_{met} = 10 nm and d_{LHM} = 9.5 nm
d_{met} = 20 nm and d_{LHM} = 19.5 nm
Field enhancement factor
Wavelength(nm)

Fig. 10. Field enhancement factors under different incidence angles θ of a transverse magnetic polarized electromagnetic field versus wavelength. (a) $\theta = 15^0$; (b) $\theta = 30^0$; (c) $\theta = 45^0$; (d) $\theta = 60^0$

4. Conclusion

This work attempts to enhance the field enhancement factor around the hydrogen/gold slab interface. The increase of this factor signifies the increase in hydrogen energy storage. We have proposed a periodic layered structure composed of n-binary unit cells based on alternating a thin layer of gold with a thin layer of the metamaterial. The effective medium theory allows us to replace this layered structure with a single slab of homogeneous material. The reflectivity spectra under different incidence angles at the hydrogen/slab interface have been deduced by the Transfer Matrix Method. The obtained field enhancement factor of the proposed model has higher values in comparison with other models for example the field enhancement factors calculated by Tanabe at the metal surfaces of Pd, Ni, and Ti in figure 2 (a) [75]. This numerical study led to the conclusion that the field enhancement factor can be boosted by minimizing: the difference between the two layers' thicknesses, the number of periods and the incidence angle.

References

[1] E.Tzimas, C. Filiou, S.D. Peteves, and J.B.Veyret, Hydrogen Storage: State-of-the-art and Future Perspective, Institute for Energy, JRC IE, PR& Communication, Européen Commission, Netherlands, 2003. ISBN : 92-894-6950-1

[2] V.A. Yartys, M.V. Lototsky, An overview of hydrogen storage methods, in: T.N. Veziroglu, S.Yu. Zaginaichenko, D.V. Schur, B. Baranowski, A.P. Shpak, V.V. Skorokhod (Eds.), Hydrogen Materials Science and Chemistry of Carbon Nanomaterials, Kluwer Academic Publ., Dordrecht 2004. 75–104. DOI: 10.1007/1-4020-2669-2_7

[3] Y.E. Cheon, & M.P Suh, Enhanced Hydrogen Storage by Palladium Nanoparticles Fabricated in a Redox-Active Metal-Organic Framework. Angewandte Chemie International Edition (2009), 48(16), 2899–2903. https://doi:10.1002/anie.200805494

[4] F. Cheng, Z. Tao, J. Liang and J. Chen, Efficient hydrogen storage with the combination of lightweight Mg/MgH2 and nanostructures. Chemical Communications (2012), 48(59), 7334–7343. doi:10.1039/c2cc30740e

[5] L. Wang, R.T. Yang, and J. Yang, Nanostructured Adsorbents for Hydrogen Storage. New and Future Developments in Catalysis (2013), 137-164. https://doi.org/10.1016/B978-0-444-53880-2.00008-9

[6] R. Zacharia and S. ullah Rather, Review of Solid State Hydrogen Storage Methods Adopting Different Kinds of Novel Materials. Journal of Nanomaterials (2015), http://dx.doi.org/10.1155/2015/914845

[7] R. Mohtadi, S. Orimo, The renaissance of hydrides as energy materials. Nature Reviews Materials (2016), 2(3), 1–15. doi:10.1038/natrevmats.2016.91

[8] M. Navlani-García, K. Mori, Y. Kuwahara and H. Yamashita, Recent strategies targeting efficient hydrogen production from chemical hydrogen storage materials over carbon-supported catalysts. NPG Asia Materials (2018), 10: 277–292. DOI 10.1038/s41427-018-0025-6

[9] M. Mohan, V.K. Sharma, E.A. Kumar, V. Gayathri, Hydrogen storage in carbon materials-a review. Energy Storage (2019), 1(2) e35. https://doi.org/10.1002/est2.35

[10] M. Hirscher, V.A. Yartys, M. Baricco, J.B. von Colbe, D. Blanchard, R.C.Jr. Bowman, D.P. Broom, C.E. Buckley, F. Chang, P. Chen, Materials for hydrogen-based energy storage—Past, recent progress and future outlook. J. Alloys Compd (2020), 827, 153548. https://doi.org/10.1016/j.jallcom.2019.153548

[11] C.J. Winter, J. Nitsch, Hydrogen as an Energy Carrier: Technologies, Systems, Economy. 1st edn. Springer Verlag, Berlin, New York 1988.

[12] C. Carpetis, Storage, transport and distribution of hydrogen, in Hydrogen as an Energy Carrier: Technologies, Systems, Economy (eds C.J. Winter and J. Nitsch), Springer Verlag, 1988, 249–290.

[13] L. Zhou, Progress and problems in hydrogen storage methods. Renewable and Sustainable Energy Reviews (2005), 9 (4), 395–408. https://doi.org/10.1016/j.rser.2004.05.005

[14] M. Ni, An Overview of Hydrogen Storage Technologies. Energy Exploration & Exploitation (2006), 24(3), 197–209. doi:10.1260/014459806779367455

[15] M. Hirscher, Handbook of Hydrogen Storage. WILEY-VCH Verlag GmbH & Co. KGaA, Weinheim 2010. ISBN: 978-3-527-32273-2.

[16] A. Godula-Jopek, W. Jehle and J. Wellnitz, Hydrogen Storage Technologies: New Materials, Transport and Infrastructure, Wiley-VCH Verlag GmbH, Weinheim 2012.

[17] S.S. Makridis, Hydrogen storage and compression (2017), arXiv: 1702.06015, DOI: 10.1049/PBPO101E_ch1

[18] G. Sandí, Hydrogen Storage and Its Limitations. Electrochemical Society Interface (2004), DOI: 10.1149/2.F06043IF

[19] R. Prabhukhot Prachi, M. Wagh Mahesh, C. Gangal Aneesh, A Review on Solid State Hydrogen Storage Material. Advances in Energy and Power (2016), 4(2), 11-22. DOI: 10.13189/aep.2016.040202

[20] R. Pedicini, I. Gatto, & E. Passalacqua, Solid-State Materials for Hydrogen Storage. Nanostructured Materials for Next-Generation Energy Storage and Conversion (2018), 443–467. doi:10.1007/978-3-662-56364-9_15

[21] E. David, An overview of advanced materials for hydrogen storage. Journal of Materials Processing Technology (2005), 162-163, 169-177. https://doi.org/10.1016/j.jmatprotec.2005.02.027

[22] M. Felderhoff, C. Weidenthaler, R. Helmolt, U. Eberle, Hydrogen storage: the remaining scientific and technological challenges. Phys. Chem. Chem. Phys (2007). doi:10.1039/b701563c.

[23] A. Züttel, Materials for hydrogen storage. Materials today (2003), 6(9), 24-33. doi:10.1016/S1369-7021(03)00922-2

[24] G. Alefeld, R.M. Cotts, K.W. Kehr, H. Kronmtiller, H. Peisl, A. Seeger, K. Skold, T. Springer, A. C. Switendick, J. Volkl, F.E. Wagner, H. Wagner, W. E. Wallace, G. Wortmann (eds.), Hydrogen in Metals I, Basic Properties, Springer-Verlag, Berlin-Heidelberg-New York, (1978).

[25] K. Christmann, Hydrogen Adsorption on Metal Surfaces. R.M. Latanision, J.R. Pickens (eds) Atomistics of Fracture. Springer, Boston, MA. 1983. https://doi.org/10.1007/978-1-4613-3500-9_12

[26] P.M. Quaino, R.Nazmutdinov, L.F. Peiretti and E. Santos. Unravelling the hydrogen absorption process in Pd overlayers on a Au(111) surface. Phys. Chem. Chem. Phys. (2016), 18(5):3659–3668. https://doi.org/10.1039/C5CP06443K

[27] G. Alefeld, B. Baranowski, H. Brodowsky, T. Schober, B. Stritzker, H. Wenzl, Ch.A. Wert, E. Wicke, H. Wipf, R. Wiswall, H. Wiihl (eds.), Hydrogen in Metals II, Application-Oriented Properties, Springer-Verlag, Berlin-Heidelberg-New York, (1978).
[28] T. Tanaka, M. Keita, & D E. Azofeifa, Theory of hydrogen absorption in metal hydrides. Phys. Rev. B (1981), 24(4), 1771–1776. https://doi:10.1103/physrevb.24.1771

[29] J. Graetz, Metastable Metal Hydrides for Hydrogen Storage. International Scholarly Research Network (2012). doi:10.5402/2012/863025

[30] V. Berube, G. Radtke, M. Dresselhaus, G. Chen, Size effects on the hydrogen storage properties of nanostructured metal hydrides: A review. International Journal of Energy Research (2007), 31(6-7), 637–663. doi:10.1002/er.1284

[31] I.P. Jain, P. Jain, & A. Jain, Novel hydrogen storage materials: A review of lightweight complex hydrides. Journal of Alloys and Compounds (2010), 503(2), 303–339. doi:10.1016/j.jallcom.2010.04.250

[32] M. Pozzo, D. Alfè, A. Amieiro, S. French, A. Pratt, Hydrogen dissociation and diffusion on Ni and Ti-doped Mg(0001) surfaces. J Chem Phys (2008), 128(9), 094703-094713. https://doi.org/10.1063/1.2835541

[33] A. Jain, S. Agarwal, T. Ichikawa, Catalytic Tuning of Sorption Kinetics of Lightweight Hydrides: A Review of the Materials and Mechanism. Catalysts (2018), 8, 651. https://doi.org/10.3390/catal8120651

[34] S. Somo, M. Maponya, D. Davids, H. Hato, L. Lototskyy, M A. Modibane, A Comprehensive Review on Hydrogen Absorption Behaviour of Metal Alloys Prepared through Mechanical Alloying. Metals (2020), 10, 562. doi:10.3390/met10050562
[35] A. Aricò, P. Bruce, B. Scrosati, J.-M. Tarascon, and W. van Schalkwijk, “Nanostructured materials for advanced energy conversion and storage devices,” Nat. Mater (2005), 148–159. doi:10.1142/9789814317665_0022

[36] S. Kishore, J.A. Nelson, J.H. Adair, P.C. Eklund, Hydrogen storage in spherical and platelet palladium nanoparticles. Journal of Alloys and Compounds (2005), 389(1–2), 234–242. https://doi.org/10.1016/j.jallcom.2004.06.105

[37] M.U. Niemann, S.S. Srinivasan, A.R. Phani, A. Kumar, D.Y. Goswami, E.K. Stefanakos, Nanomaterials for hydrogen storage applications: A review. J. Nanomater (2008), 1–9. doi:10.1155/2008/950967.

[38] Q. Luo, J. Li, B. Li, B. Liu, H. Shao, & Q. Li, Kinetics in Mg-based hydrogen storage materials: Enhancement and mechanism. Journal of Magnesium and Alloys (2018). doi:10.1016/j.jma.2018.12.001

[39] A. Schneemann, J. L. White, S. Kang, S. Jeong, L.F. Wan, E.S. Cho, … V. Stavila, Nanostructured Metal Hydrides for Hydrogen Storage. Chemical Reviews. (2018) https://doi:10.1021/acs.chemrev.8b00313

[40] T.K. Nielsen, M. Polanski, D. Zasada, P. Javadian, F. Besenbacher , J. Bystrzycki, … T. R. Jensen, Improved Hydrogen Storage Kinetics of Nanoconfined NaAlH4 Catalyzed with TiCl3 Nanoparticles. ACS Nano (2011), 5(5), 4056–4064. doi:10.1021/nn200643b

[41] M.L. Christian and K. F. Aguey-Zinsou, Core−shell strategy leading to high reversible hydrogen storage capacity for NaBH4. ACS Nano (2012), 6(9), 7739–7751. doi:10.1021/nn3030018

[42] Y. Li, Z. Zhou, P. Shen, S.B. Zhang and Z. Chen, Computational studies on hydrogen storage in aluminum nitride nanowires/tubes. Nanotechnology (2009), 20(21), 215701 doi:10.1088/0957-4484/20/21/215701

[43] A. Baldi and B. Dam, Thin film metal hydrides for hydrogen storage applications. J. Mater. Chem. (2011), 21(12), 4021–4026. https://doi:10.1039/c0jm03249b

[44] Y. Nishijima, S. Shimizu, K. Kurihara, Y. Hashimoto, H. Takahashi, A. Balcytis, G. Seniutinas, S. Okazaki, J. Juodkazyte, T. Iwasa, T. Taketsugu, Y. Tominaga, and S. Juodkazis, Optical readout of hydrogen storage in films of Au and Pd. OPTICS EXPRESS (2017), 25(20) 24081. doi:10.1364/oe.25.024081

[45] W.L Watkins and Y. Borensztein, Mechanism of hydrogen adsorption on gold nanoparticles and charge transfer probed by anisotropic surface plasmon resonance. Phys. Chem. Chem. Phys. (2017), 19(40), 27397–27405. doi:10.1039/c7cp04843b

[46] K. Higuchi, H. Kajioka, K. Toiyama, H. Fujii, S. Orimo, & Y. Kikuchi, In situ study of hydriding–dehydriding properties in some Pd/Mg thin films with different degree of Mg crystallization. J. Alloys Comp. (1999), 293-295, 484-489. https://doi:10.1016/s0925-8388(99)00470-3

[47] K. Higuchi, K. Yamamoto, H. Kajioka, K. Toiyama, M. Honda, S. Orimo, H. Fujii, Remarkable hydrogen storage properties in three-layered Pd/Mg/Pd thin Films. J Alloys Compds (2002), 330-332, 526–530. doi:10.1016/s0925-8388(01)01542-0

[48] R. Bell, The effect of microwave fields on the interaction of hydrogen with hydride forming materials, PhD thesis, University of Birmingham. Eng.D., 2015.

[49] J-Y. Hwang, S. Shi, X. Sun, Z. Zhang, C. Wen, Electric charge and hydrogen storage. Int J Energy Res. (2011), 37:741-745. https://doi.org/10.1002/er.1856.

[50] A. Borgschulte, J.H. Rector, H. Schreuders, B. Dam, & R. Griessen, Electrohydrogenation of MgH_2-thin films. Applied Physics Letters (2007), 90(7), 071912. https://doi:10.1063/1.2695626

[51] E H. Song, S H. Yoo, JJ. Kim, SW. Lai, Q. Jiang, SO. Cho, External electric field induced hydrogen storage/release on calcium decorated single-layer and bilayer silicene. Phys Chem Chem Phys (2014), 16:23985-92.

[52] S. Guo, C. Hu, H. Zhang, Unidirectional ultrabroadband and wide-angle absorption in graphene-embedded photonic crystals with the cascading structure comprising the Octonacci sequence. J. Opt. Soc. Am. B (2020), 37, 2678–2687.

[53] Y. Xu, B. Wan, Z. Zhou, Y. Ma, H. Zhang, and D. Zhang, Tunable and asymmetric optical bistability of one-dimensional photonic crystals based on InSb and nonlinear materials. Applied Optics (2020), 59, 31.

[54] N. Fukuoka, K. Tanabe, Large plasmonic field enhancement on hydrogen-absorbing transition metals at lower frequencies: Implications for hydrogen storage, sensing, and nuclear fusion. J. Appl. Phys (2019), 126(2), 023102. https://doi:10.1063/1.5091723

[55] O. Sakai and K. Tachibana, Plasmas as metamaterials: a review. Plasma Sources Sci. Technol (2012), 21, 013001.

[56] Hai-Feng Zhang, The band structures of three-dimensional nonlinear plasma photonic crystals, AIP Adv (2018), 8, 015304.

[57] V. Veselago, The electrodynamics of substance with simultaneously negative index values of ε and μ, Soviet Physics Uspekhi. (1968), 10(4), p. 509-514.

[58] V. Veselago, L. Braginsky, V. Shklover and C. Hafner, Negative Refractive Index Materials. Journal of Computational and Theoretical Nanoscience (2006), 3(2):189-218.

[59] B. Banerjee, An Introduction to Metamaterials and Waves in Composites. Taylor & Francis Group, London, 2011. https://doi.org/10.1201/b11814

[60] R. Marqués, F. Martin and M. Sorolla, Metamaterials with Negative Parameters Theory, Design, and Microwave Applications. John Wiley & Sons, New Jersey, 2008.

[61] W. Cai and V. Shalaev, Optical Metamaterials Fundamentals and Applications, Springer, London, 2010.

[62] J.B. Pendry, Negative Refraction Makes a Perfect Lens. Physical Review Letters (2000), 85(18), 3966–3969. doi:10.1103/physrevlett.85.3966

[63] D.R. Smith, J.B. Pendry and M.C. K. Wiltshire, Metamaterials and Negative Refractive Index. Science, New Series. 2004, 305(5685)

[64] L. J. Mendoza Herrera, D. M. Arboleda, D.C. Schinca, L. B. Scaffardi, Determination of plasma frequency, damping constant, and size distribution from the complex dielectric function of noble metal nanoparticles. J. Appl. Phys. (2014), 116, 233105‑8. doi: 10.1063/1.4904349

[65] T.H. Isaac, W.L. Barnes, & E. Hendry, Determining the terahertz optical properties of subwavelength films using semiconductor surface plasmons. Appl Phys Lett (2008), 93(24), 241115. https://doi:10.1063/1.3049350

[66] J. Humlicek, Data Analysis for Nanomaterials: Effective Medium Approximation, Its Limits and Implementations. In Ellipsometry at the Nanoscale. DOI: 10.1007/978-3-642-33956-1_3

[67] V. M. Agranovich and V. E. Kravtsov, Notes on crystal optics of superlattices, Solid-State Commun (1985), 55(1). https://doi.org/10.1016/0038-1098(85)91111-1

[68] D. R. Smith and D. Schurig, Electromagnetic wave propagation in media with indefinite permittivity and permeability tensors, Phys. Rev. Lett. (2003), 90(7), 077405. https://doi.org/10.1103/PhysRevLett.90.077405

[69] P. Markoš and C. Soukoulis, Wave Propagation, From Electrons to Photonic Crystals and Left-Handed Materials. 1st edition, Princeton University Press, New Jersey, 2008. pp. 275-278

[70] X.Y. He, Q.J. Wang, & S.F. Yu, Investigation of Multilayer Subwavelength Metallic-Dielectric Stratified Structures. IEEE J Quantum Electron (2012), 48(12), 1554–1559. https://doi:10.1109/jqe.2012.2219504

[71] A. Poddubny, I. Iorsh, P. Belov, Y. Kivshar, Hyperbolic metamaterials. Nat. Photonics (2013), 7, 948–957. https://doi.org/10.1038/nphoton.2013.243

[72] H. Raether, Surface plasmons on smooth and rough surfaces and on gratings. Springer, Berlin, 1988.

[73] V.G. Kravets, A.V. Kabashin, W.L. Barnes, A.N. Grigorenko, Plasmonic Surface Lattice Resonances: A Review of Properties and Applications. Chem. Rev. (2018), 118, 5912. DOI: 10.1021/acs.chemrev.8b00243

[74] W.H. Weber, & G.W. Ford, Optical electric-field enhancement at a metal surface arising from surface-plasmon excitation. Optics Letters. (1981), 6(3), 122. https://doi:10.1364/ol.6.000122

[75] K. Tanabe, Plasmonic Field Enhancement on Planar Metal Surfaces for Condensed Matter Nuclear Fusion. Journal of Condensed Matter Nuclear Science (2018), 27 152–157.

[76] H. Hamouche, & M.M. Shabat, Field Enhancement Factor Around Hydrogen-Negative Index Metamaterial Waveguide. In: Khellaf A. (eds) Advances in Renewable Hydrogen and Other Sustainable Energy Carriers. Springer Proceedings in Energy. Springer, Singapore. 2021, https://doi.org/10.1007/978-981-15-6595-3_56

[77] G. Hass, Physics of Thin Films Advances in Research and Development, Academic Press, New York and London, 1963. pp. 69-81

[78] H. Hamouche, & M.M. Shabat Enhanced absorption in silicon metamaterials waveguide structure. Appl Phys A. (2016), 122(7). https://doi:10.1007/s00339-016-0206-5

[79] H. Hamouche, M.M. Shabat and D. M. Schaadt, Multilayer solar cell waveguide structures containing metamaterials, Superlattices and Microstructures (2017), Vol.101, http://dx.doi.org/10.1016/j.spmi.2016.08.047

[80] H. Hamouche, & M.M. Shabat, Artificial Metamaterials for High Efficiency Silicon Solar Cells. In: Benmounah A, Brahim S, Saidi M. (eds) Proceedings of the Third International Symposium on Materials and Sustainable Development. Springer Nature Switzerland. 2018, 105–115. http://doi:10.1007/978-3-319-89707-3_13

[81] H. Hamouche, & M.M. Shabat Periodic silicon nitride-metamaterials structure for enhanced solar cell efficiency. 2020 International Conference on Promising Electronic Technologies (ICPET) **DOI:** 10.1109/ICPET51420.2020.00029